*36th EPS Conference on Plasma Phys. Sofia, June 29 - July 3, 2009 ECA Vol.**33E**, P-2.157 (2009)*

Type-I ELM filamentary heat load patterns on the divertor target at JET

S. Devaux[1], T. Eich[1], G. Arnoux[2], W. Fundamenski[2], H. Thomsen[1], S. Jachmich[3], P.J. Lomas[2], E. De la Luna[4], I. Nunes[5], G.Saibene[6] and JET-EFDA Contributors*

JET-EFDA, Culham Science Center, Culham, OX14 3DB, UK
[1] Max-Planck-Institut für Plasmaphysik, EURATOM-Assoziation, Garching, Germany
[2] EURATOM-UKAEA Fusion Association, Culham Science Centre, United Kingdom
[3] Laboratory for Plasma Physics, Ecole Royale Militaire, EURATOM-Association "Belgian State", Brussels, Belgium, Partner in the Trilateral Euregio Cluster (TEC)
[4] Laboratorio Nacional de Fusión, Asociación EURATOM-CIEMAT, Madrid, Spain
[5] Instituto de Plasmas e Fusão Nuclear, Associação EURATOM-IST, Lisboa, Portugal
[6] FUSION FOR ENERGY, Joint Undertaking, 08019 Barcelona, Spain
∗ See Appendix of F.R.Romanelli et al., Fusion Energy 2008 (Proc. 22nd Int. Conf. Geneva, 2008) IAEA 2008

Type-I ELMs are quasi-periodic events associated with H-mode plasma operations during which energy is suddenly released from the pedestal region. A large fraction of this energy is driven onto the divertor target tiles via parallel transport along magnetic field lines. The resulting heat load pattern exhibits spatially spaced striations (Fig. 1), interpreted as the footprints of the filamentary structure of ELMs [1]. The large variability of patterns observed as well as their displacement with outer strike point position (OSP) make clear that these striations are not due to layers on the target. A new infrared camera installed at JET has been used to study the dynamic and spatial structure of heat load on divertor targets during type-I ELMy H-mode. Its high spatial resolution (1.7mm on outboard target) and frame rate frequency f_{IR} ($1/f_{IR}$ down to $35\mu s$) allow an accurate study of striations caused by the filamentary nature of type-I ELMs seen on the divertor target tiles [2]. A simple model based on transport on the scrape-off layer has been developed in order to mimic the striations.

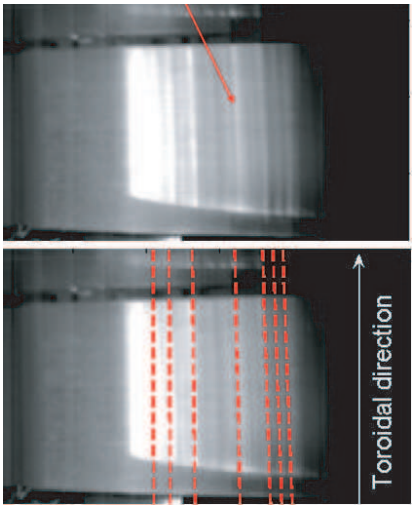

Figure 1: Striations observed during type-I ELM on the outer target match the intersection of B field lines with the target (red curves).

Modelling of ELM striations

From pre-ELM equilibrium magnetic reconstruction, it is possible to map the magnetic field lines starting at the outer midplane on the divertor plate (Fig. 2). It appears that striations observed (Fig. 1) at different radial positions on the target start at different toroidal locations at the midplane. To model these striations, we assume that during an ELM, particles are radially released at the outer midplane and crossed the magnetic field lines at a constant velocity $v_{\perp}$.

Then, they reach the divertor targets strictly following the magnetic field lines. Power load on the outer target P_o^{ELM}, derived from a model discussed in [4] where a free-streaming approach is assumed for particles released, is given by:

$$P_o^{ELM}(t) = \frac{2}{3}\frac{E^{ELM}}{\sqrt{\pi}} \times \left(1 + \left(\frac{\tau_\perp + \tau_{//}}{t}\right)^2\right) \times \frac{\tau_\perp + \tau_{//}}{t^2} \times \exp\left(-\left(\frac{\tau_\perp + \tau_{//}}{t}\right)^2\right) \quad (1)$$

where E^{ELM} is the overall ELM target deposited energy, $\tau_\perp = r_{mid}/v_\perp$ is the time required to reach the field line located at r_{mid} from the separatrix at the midplane and $\tau_{//} = L_c/c_s$ is the typical parallel transport time along field lines. The sound speed c_s is estimated with the pedestal top electron temperature prior to ELM event and the connection length to the midplance L_c, which monotically decreases with major radius R (37m at 1cm from the outer strike point (OSP) down to 20m at the edge of the tile, 10cm far from the OSP) is obtained from pre-ELM equilibrium magnetic reconstruction. The heat deposition on the target associated with each single filament is modeled with a gaussian distribution with a full width at half maximum $\delta\phi \approx 50°$, based on the radial width of the striations measured on the target (Fig. 3).

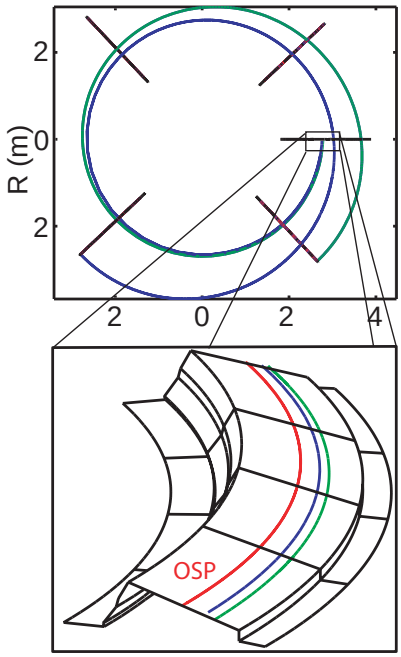

Figure 2: Mapping of B-field lines shows that striations seen at different radial position start at different toroidal angles at the midplane.

Without further assumptions, the model is not able to reproduce experimental patterns. Time required by filaments to reach the target is only determined by perpendicular transport at the midplane and parallel transport along field lines, so that simulated profiles are always identical when experimental patterns show a large variability. Experiment shows that the first striation observed during one ELM appears at a random location on the target, without respect to $\tau_\perp + \tau_{//}$. This led us assume that not all particles are leaving the outer midplane at the same time (compatible with a recent analysis on JET [5]). As a consequence a random delay has been introduced in the model, allowing filaments to start at different times: arrival on the target now depends on both delay and transport time, so that the first striation can appear at every locations of the tile.

Comparison with experiment

In order to test our model we have compared experimental data with numerically generated heat profiles. Experimental data are from discharges where ELMs losses are around 8% of the plasma stored energy (for a core density of 6.10^{19}.m^{-3} and 17MW of input power). For a typical pedestal electron temperature $T_e \approx 1keV$, simulated profiles show the best agreement for a value

of $v_\perp$ between 500m.s^{-1} - 1km.s^{-1} and a maximum random delay set to 70μs. These settings are also compatible with results from [5].

One simulated heat flux profile obtained for striations with a mode number of 20 is shown on Fig. 4. The agreement between simulated and experimental profiles is good, as striation locations on the tile and time evolution are correctly reproduced. However, the early presence of striations very close to the OSP is not reproduced by the model. Moreover, simulated striations obtained in this area are very close to each other and are quite small in contrast to experiment (Fig.3a). These two findings suggest that some phenomena not taken into account affect the dynamics along field lines near the OSP.

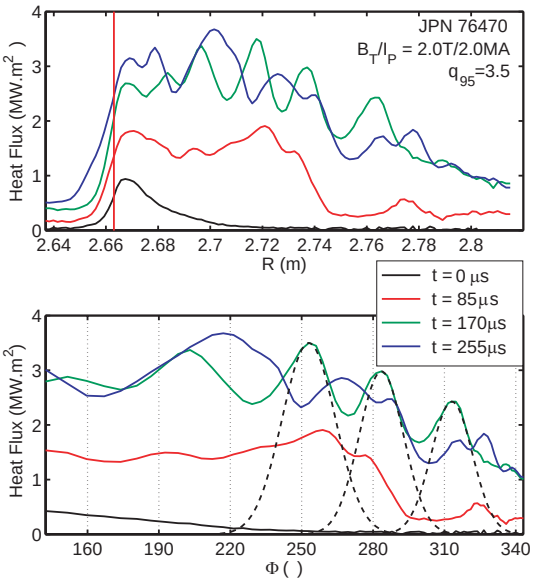

Figure 3: a. Experimental heat flux profile on the outer target during Type-I ELM. b. Heat profiles plotted against toroidal angle at the midplane Φ.

Mode number analysis

To a striation observed at a given radial position on the target corresponds a given toroidal location Φ_i of the source at the outer midplane. A quasi toroidal mode number (QMN) is derived from the toroidal distribution of the s sources such that:

$$n_{QMN} = \frac{1}{s}\sum_{j=1}^{s}\frac{2\pi}{\Phi_j - \Phi_{j+1}}. \qquad (2)$$

When studying striations at τ_{IR}, time corresponding to the maximum of power deposition on target during one ELM, one can find that less striations than expected are observed on the target (as s should be equal to n_{QMN}). In the present case (Fig.3a (blue curve)), only 13 striations (extrapolated to 360°) are found for a QMN $\approx$ 20. The missed striations presumably are in the vicinity of the OSP, where profiles are perturbed and striations no more identified.

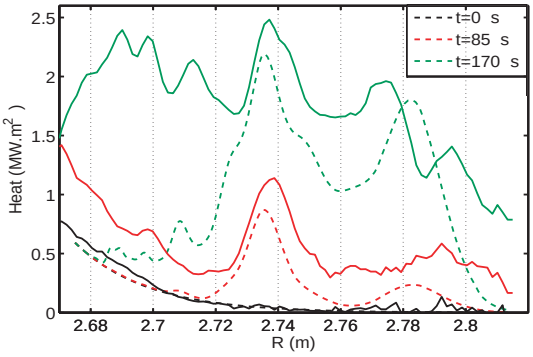

Figure 4: Simulated (dashed lines) and experimental (plain lines) heat profiles on the outer target for 2 consecutive times during a type-I ELM.

Fig. 3a also shows that s, the number of observed striations, and its associated QMN increase during ELM event. The evolution of both s and n_{QMN} have been systematically studied over 115 ELMs in a JET pulse, with a time resolution $1/f_{IR} = 41\mu s$. Fig. 5a shows n_{QMN} as a function of the time (relative to the ELM event) normalized to τ_{IR}. The heat load distribution during the rise of ELMs can be divided into two stages. First, n_{QMN} increases from 4 to 20 (in average)

within a time interval corresponding to $0.4\tau_{IR}$. s varies together with n_{QMN} and both quantities saturate at the end of the first stage. During the second phase, power deposition on the tile still increases but, s and n_{QMN} staying constant, this increase is only due to an increasing amount of energy carried by each single filaments.

Fig5b shows QMN evolution from 115 simulated ELMs, where heat profiles have been obtained with 13 striations dispatched on the tile as expected for a QMN of 20. The rising time of ELM has been set to $200\mu s$ and the maximum delay to $70\mu s$. The two phases depicted earlier are also visible on the numerical profiles, with comparable starting value for n_{QMN}, which reinforce our confidence in the model.

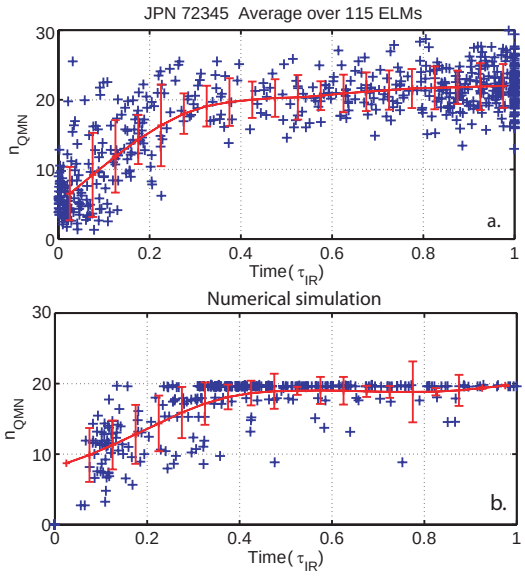

Figure 5: Time evolution of n_{QMN} normalized to τ_{IR} from experiment (a) and simulation (b).

This agreement between model and experiment allows us to give an interpretation of the increasing of QMN. It has already been established that the time required by particles to reach the wall differs from one striation to the other, so that the increasing of s with time is well understood. Consequence of the delay between starting time of filaments is that striations appears randomly on the target: the probability that the two first striations appear side by side is low. The measured QMN is then lower than the expected 20, and increases with the arrival of new filaments. Its maximum and actual value is reached when all striations are seen on the target.

Further work will investigate the impact of plasma parameters such as q_{95} on the QMN reached at the maximum of ELMs. Value derived for $v_{\perp}$ et random delay will also be investigating for different size of ELM and compare to ones found by other analysis.

This work, supported by the European Communities under the contract of Association between EURATOM/IPP, was carried out within the framework of the European Fusion Development Agreement. The views and opinions expressed herein do not necessarily reflect those of the European Commission.

References

[1] A. Kirk *et al.* Phys. Rev. Lett. **92**, 245002 (2004)
[2] T. Eich *et al.*, Phys. Rev. Lett. **91**, 195003 (2003)
[3] T. Eich *et al.*, Plasma Phys. Control. Fus **91**, 815 (2005)
[4] W. Fundamenski *et al.*, Plasma Phys. Control. Fus. **48**, 109 (2006)
[5] C. Silva *et al.*, Plasma Phys. Control. Fus., *to be submitted*